Bull. Mater. Sci., Vol. 39, No. 7, December 2016, pp. 1827–1834. © Indian Academy of Sciences.
DOI 10.1007/s12034-016-1326-4

Microstructure and wear behaviour of FeAl-based composites containing *in-situ* carbides

RAVI KANT[1,*], UJJWAL PRAKASH[1], VIJAYA AGARWALA[1] and V V SATYA PRASAD[2]
[1]Department of Metallurgical and Materials Engineering, IIT Roorkee, Roorkee 247 667, India
[2]Defence Metallurgical Research Laboratory, Kanchanbagh, Hyderabad 500 058, India

MS received 17 February 2016; accepted 25 April 2016

Abstract. **Iron aluminides containing carbon are promising materials for tribological applications. Because of graphite formation at higher (>20 wt%) Al-contents the addition of carbon to FeAl-based alloys has not been successful. The graphite precipitation may be avoided by addition of Zr or Ti. Dry sliding wear behaviour of FeAl-based alloys containing 1–1.5 wt% carbon with quaternary addition of Ti or Zr has been studied using ball-on-disk wear test. Effect of sliding speeds and applied loads is investigated and correlated with mechanical properties. Wear resistance of FeAl-based alloys is found to be significantly improved on addition of Ti/Zr. This is attributed to the high hardness of alloy carbides. The lower load-bearing capacity of graphite flakes in localized region was found to increase the wear rate of the alloy. The carbides such as $Fe_3AlC_{0.5}$, TiC and ZrC are embedded in the matrix after sliding wear without destruction or delamination. This significantly affects the wear resistance of FeAl-based alloys.**

Keywords. **FeAl-based composites; precipitation; mechanical properties; wear.**

1. Introduction

Fe–Al alloys are potential material for tribological applications because they have good wear resistance and high-temperature strength [1,2]. Recently, different studies showed that the carbon addition may improve the strength, creep resistance, machinability, wear resistance and resistance to environment embrittlement [3–5]. Among the Fe–Al alloys, FeAl with ordered B2 structure shows better wear resistance as compared with Fe_3Al and α-Fe [6]. However, in B2 FeAl alloys, carbon addition leads to a loss in the strength [7,8]. This is attributed with the precipitation of soft graphite phase. Graphite precipitation may be prevented by addition of strong carbide formers such as Ti, Zr and Cr [9,10].

It has been reported that Ti addition to Fe_3Al and FeAl alloys effectively reduced the wear rate and coefficient of friction [11–13]. Further Ti addition is found to increase the yield strength and creep resistance at higher temperature [14]. Zr addition may be of interest because of very low solid solubility in Fe–Al alloys and effectiveness in the increase in the strength due to precipitation of Laves phase [15,16]. In FeAl alloys containing carbon, Ti/Zr addition may lead to formation of TiC/ZrC, thus forming a composite with the FeAl matrix.

Intermetallic alloys reinforced by carbide particles may exhibit superior wear resistance due to higher hardness of carbides [6,12,17,18]. However, interface bonding between particles and matrix is always an issue in composites fabricated through the powder metallurgy routes [19]. In composites prepared by melting and casting, *in-situ* carbides formation results in strong atomic bonding between carbides and matrix [20–22]. The present work studies the composites prepared by addition of Ti and Zr addition to B2 FeAl alloys containing carbon and the wear behaviour of alloys is correlated with mechanical properties.

2. Experimental

The FeAl-based alloys received were prepared by argon arc melting using commercially pure iron (99%), aluminium (99.99%), titanium (99.8%) or zirconium to produce pancakes of 75-mm diameter and 10-mm thickness. The nominal compositions of alloys studied are listed in table 1. For microstructural characterization, specimen sections were ground to 1500 grit and polished with alumina powder (0.5 μm). The polished samples were etched with etchant composed of 33% CH_3COOH + 33% HNO_3 + 33% H_2O + 1% HF by volume. A scanning electron microscope (FEI Qunta 200 F) equipped with energy dispersion spectroscopy (EDS) was used to study the polished samples. The volume fractions of different phases were measured using Dwinter material plus software. The phases present in different specimen were identified using EDS and XRD. For XRD studies on polished samples, an X-ray diffractometer (D8-Advance Bruker-axe) was used with Cu K_α radiation ($\lambda = 1.5405$). The bulk hardness of the alloys was measured using a FIE-VM50 PC Vickers hardness tester at a load of 10 kg. The microhardness of different phases was measured using a load of 25 g in a VHM-002 Walter UHL hardness tester. The compressive test specimens of 6-mm diameter and 9-mm length

*Author for correspondence (kravidmt@iitr.ac.in)

Table 1. Nominal composition and volume fraction of different phases of alloys.

Compositions (wt%)					Volume fraction of various phases (%)				
Alloys	Al	C	Ti or Zr	Fe	Graphite	$Fe_3AlC_{0.5}$	TiC	ZrC	$Zr(Fe,Al)_2$
Alloy-1	22.0	1.0	—	Balance	<3.0	12–14	—	—	—
Alloy-2	22.0	1.0	5.0 (Zr)	Balance	—	—	—	11–13	6–8
Alloy-3	22.0	1.0	5.0 (Ti)	Balance	—	—	14–17	—	—
Alloy-4	22.0	1.5	5.0 (Ti)	Balance	—	—	20–23	—	—

were cut from the ingots by electro-discharge machining. The tests were performed using an S-series H75K-S tensile testing machine at a constant strain rate of 10^{-4} s^{-1} at room temperature.

The dry sliding wear tests were carried out using a ball-on-disc apparatus. Specimens with size of $12 \times 12 \times 5$ mm^3 were used. The specimen was polished with different grades of emery papers and then finally cloth polished using 0.5-μm grade alumina powder finish. The surface roughness of polished and wear surfaces was measured using a surface profiler (Mytutoyo SJ-400, Japan). SiC balls (6-mm diameter and hardness 25–28 GPa) were used as the counter-material. The wear tests were conducted at different sliding speeds of 0.1, 0.21 and 0.31 m s^{-1} to the total distance of 124, 252 and 377 m. The applied loads were 5, 10 and 20 N with testing time of 20 min. Three different wear tracks with diameters 4, 8 and 12 mm were used for each specimen. The wear rate was evaluated by dividing the volume of the wear scar by the load and the sliding distance. The depth of wear track of various specimens was also measured with the profiler. Averages of three different readings were taken. The friction force and coefficient of friction were obtained automatically. The morphologies of worn surfaces of all the samples were studied using scanning electron microscopy (SEM) to understand the wear mechanism.

3. Results and discussion

3.1 *Microstructural characterization*

Microstructure of Alloy-1 exhibits three phases. These phases are identified in figure 1 as FeAl (matrix), graphite with dark star shape (region A) and $Fe_3AlC_{0.5}$ phase (region B), which forms a continuous network at the FeAl grain boundaries. $Fe_3AlC_{0.5}$ precipitate is observed to have an average width of 5 μm. The average width and length of the graphite flake is found to be ∼3 and 55 μm, respectively. EDS results show that the region B comprises Fe, Al and C. Alloy-2 (figure 2) consists of cuboid-shaped ZrC (region C), an FeAl matrix and fine precipitates (region D) at the grain boundaries. The average edge size of ZrC carbides is found to be ∼10 μm. The results of EDS analysis reveal that cubiod-shaped particle (region C) is comprised of Zr and C, whereas particles along the grain boundaries show the presence of Zr, Al and Fe and may be the Laves phase $Zr(FeAl)_2$.

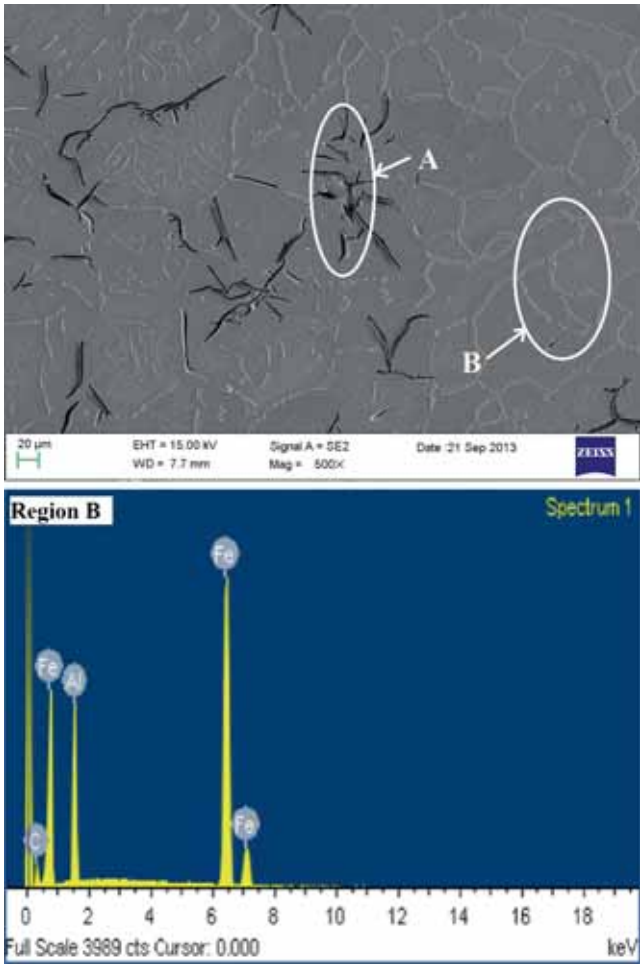

Figure 1. SEM micrographs and EDS analysis of carbides of Alloy-1 with network structure of graphite flakes (region A) and $Fe_3AlC_{0.5}$ carbides (region B).

Alloy-3 (figure 3a) exhibits three phases with cuboid-shaped TiC (region E) and elongated $Fe_3AlC_{0.5}$ (region F) in FeAl matrix. The average edge size of TiC is ∼15 μm, while the average width and length of $Fe_3AlC_{0.5}$ carbide is found to be ∼2 and ∼20 μm, respectively. A similar microstructure is obtained for Alloy-4 (figure 3b) where only the carbon content is increased from 1.0 to 1.5 and hence the volume fraction and size of carbides are found to increase. The average edge size of TiC is ∼25 μm, whereas the average width and length of $Fe_3AlC_{0.5}$ carbide are found to be ∼2 and ∼30 μm,

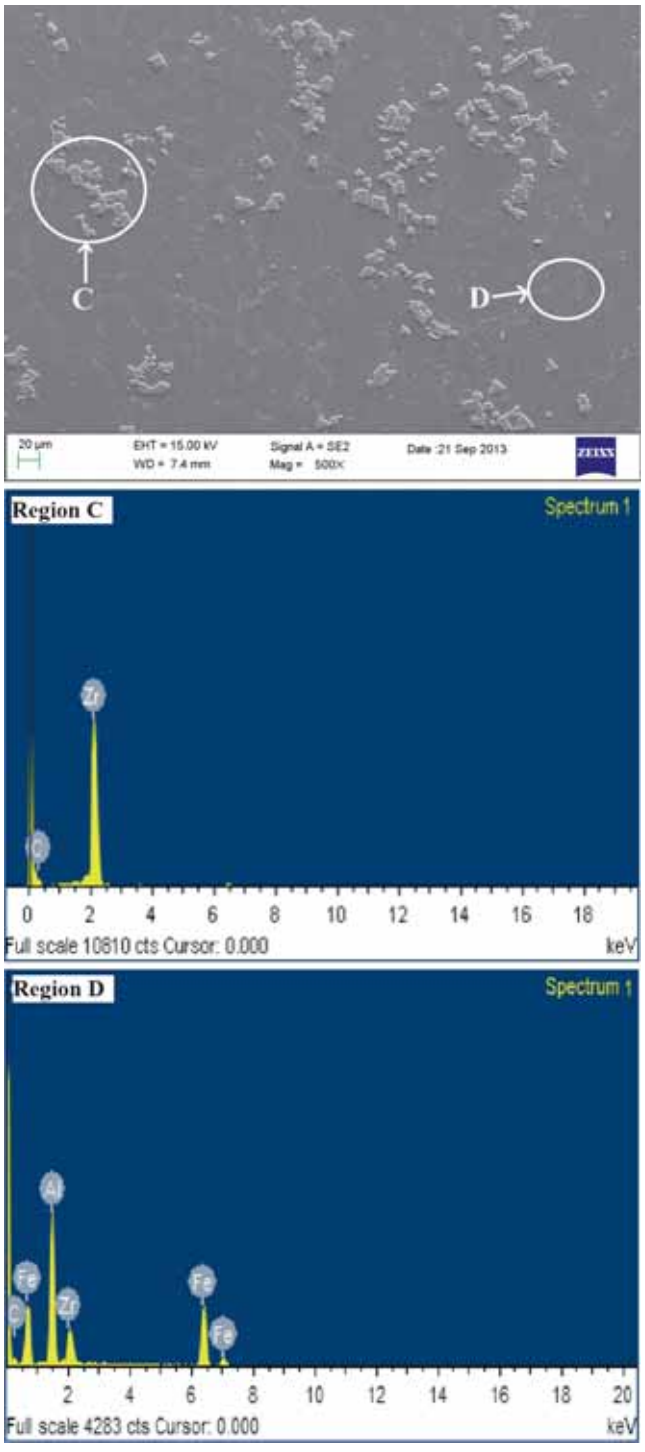

Figure 2. SEM micrographs and EDS analysis of carbides of Alloy-2 with cuboid ZrC (region C) and Laves phase $Zr(FeAl)_2$ (region D).

respectively. EDS results reveal that the cuboid-shaped particle (region E) is composed of Ti and C and elongated one (region F) comprises of Fe, Al and C. The volume fraction of different carbides increased with increase in the carbon content as given in table 2.

The XRD patterns of alloys are shown in figure 4. XRD pattern of Alloy-1 confirms the presence of $Fe_3AlC_{0.5}$ with

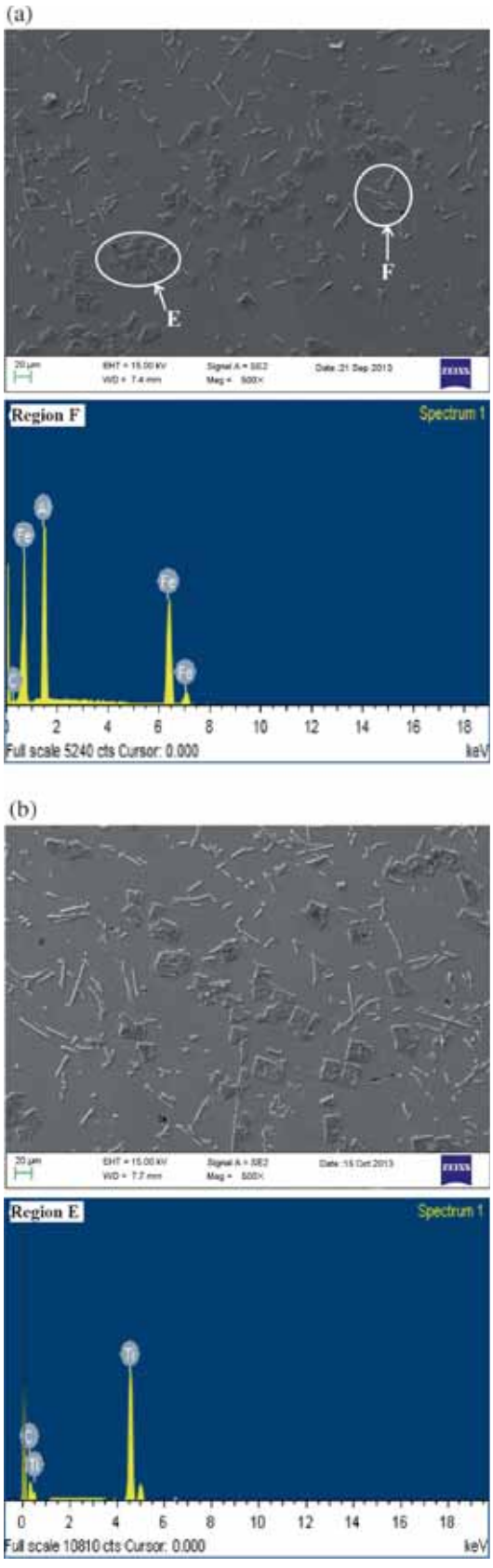

Figure 3. SEM micrographs and EDS analysis of carbides of **(a)** Alloy-3 with cuboid TiC (region E) and elongated $Fe_3AlC_{0.5}$ carbide particles (region F) and **(b)** Alloy-4 with similar carbide particles.

Table 2. Bulk hardness, microhardness and compressive strength of various alloys listed below.

Alloys	Bulk hardness (Hv)	Microhardness values (Hv)			Compressive yield strength (MPa)
		Matrix	$Fe_3AlC_{0.5}$	TiC or ZrC	
Alloy-1	385	350	600	—	900
Alloy-2	400	380	—	2650	1000
Alloy-3	425	410	610	3000	1050
Alloy-4	470	410	610	3000	1200

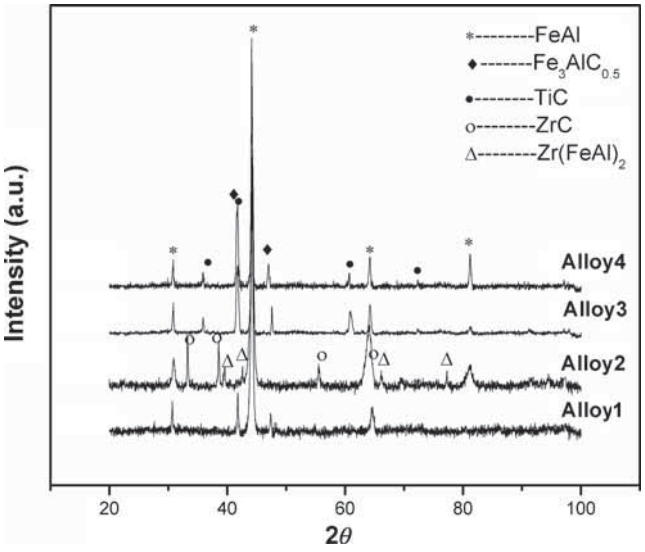

Figure 4. XRD patterns obtained from all FeAl-based alloys.

ordered B2 FeAl matrix. The peaks of graphite in Alloy-1 are not observed in the XRD pattern (figure 4), indicating that the volume fraction of graphite is low (<3%). In Alloy-2, XRD indicates the presence of ZrC carbides, a few peaks of Laves phase $Zr(Fe,Al)_2$ and ordered B2 FeAl matrix. The presence of TiC and $Fe_3AlC_{0.5}$ with ordered B2 FeAl matrix in Alloy-3 and Alloy-4 is also confirmed by XRD analysis as shown in figure 4.

All alloys exhibit FeAl-based matrix with B2 ordered structure. Both Zr and Ti have affinity to C and from ZrC/TiC, thus preventing the formation of graphite. No $Fe_3AlC_{0.5}$ carbides were observed in Alloy-2. SEM images of these alloys were used to calculate the volume fraction of various phases observed (table 1). The software was unable to distinguish $Fe_3AlC_{0.5}$ and TiC carbides in Alloy-3 and Alloy-4 and therefore a combined carbide volume fraction is reported.

3.2 *Mechanical properties*

3.2a *Hardness and compression*: The mechanical properties of alloys are given in table 2. An average of three tests was taken to determine these values. Alloy-1 exhibits low strength and hardness because of the graphite present in the alloy. Alloy-2 and Alloy-3 exhibit comparable values of strength and hardness but higher than those of Alloy-1 due to the presence of hard ZrC and TiC carbides, respectively.

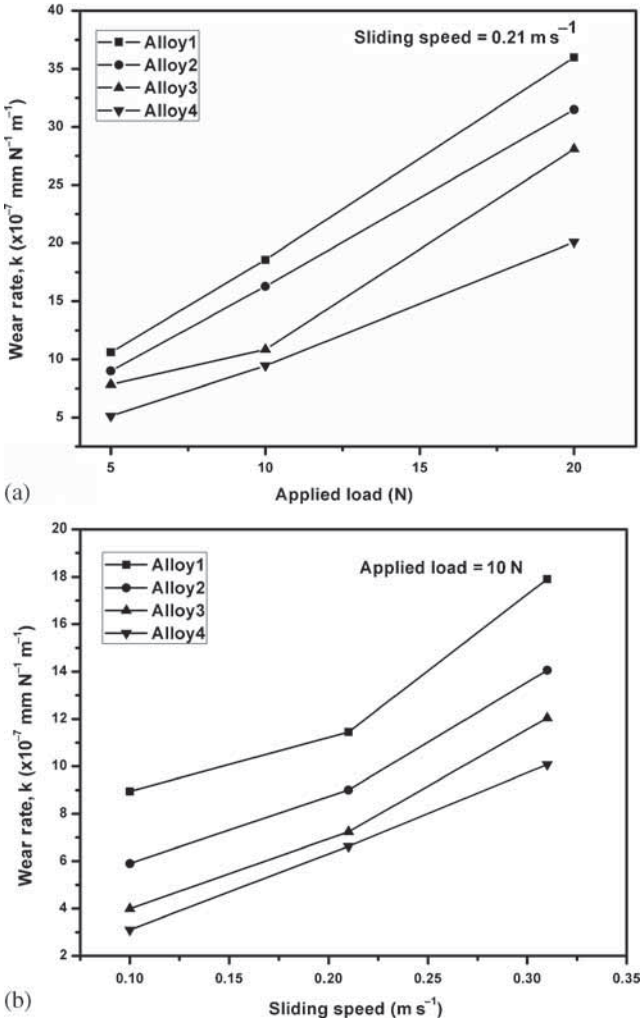

Figure 5. The variation of wear rate of FeAl-based alloy: **(a)** applied loads and **(b)** sliding speeds.

In Alloy-2 and Alloy-3, the matrix hardness also shows some improvement due to limited solubility of Zr/Ti in FeAl [10,23]. There is no change in matrix hardness on increasing the carbon content from 1% (Alloy-3) to 1.5% (Alloy-4), indicating that no further carbon has gone into the matrix. ZrC and TiC precipitates have higher values of hardness than that of $Fe_3AlC_{0.5}$. Lower volume fraction of carbides results in lower strength and hardness in Alloy-2 compared with Alloy-3. Alloy-4, which has the highest carbon (and carbide) content, exhibited the highest values of hardness and strength. Thus strength of these alloys is determined by the volume fraction and hardness of carbides present.

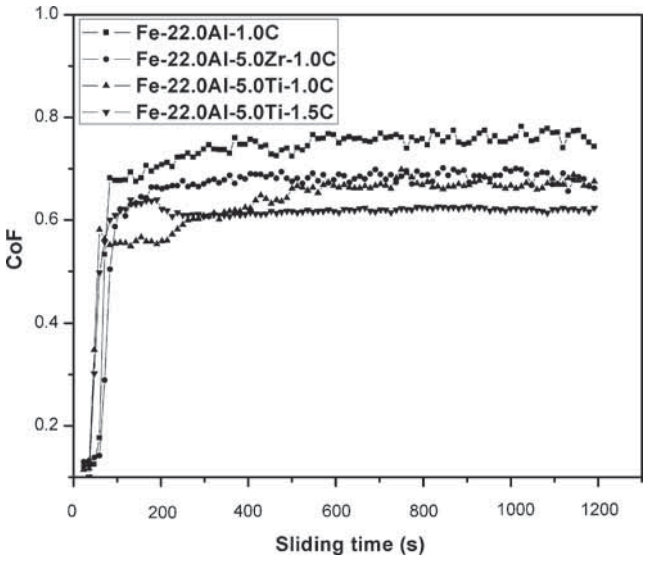

Figure 6. The variation of coefficient of friction (CoF) with time for FeAl-based alloys at applied load 10 N with sliding speed 0.21 m s^{-1}.

3.2b *Wear*: Wear rate from wear test of FeAl-based alloys is plotted *vs.* applied load at different sliding speeds. The wear rate k (mm^3 $(Nm)^{-1}$) is given by

$$k = \Delta V / FS, \tag{1}$$

where ΔV is the volume loss (mm^3), F the applied load (N) and S the sliding distance (m).

The wear rate increases as applied load increases (figure 5a). Alloy-1 shows the highest wear rate among the alloys. Alloy-2 has a moderate wear rate. Alloy-3 and Alloy-4 with the same Ti content show significant wear rate difference under the given test conditions. Among all the alloys, Alloy-4 shows the lowest wear rate. During sliding wear, the surface of the material is removed initially and load is mainly transferred to the carbide particles. Thus, the hardness of the carbide particles plays an important role under the applied load. Carbides with high hardness (here TiC) lead to lower wear rate.

The wear rate of FeAl-based alloys is plotted as a function of the sliding speed in figure 5b. The wear rate increases with higher speed. Alloy-1 shows the highest wear rate. Alloy-3 and Alloy-4 show less wear rate difference at slow speed but the difference becomes significant at higher speed with Alloy-3 exhibiting higher wear rate than that of Alloy-4. Alloy-4 exhibits the lowest wear rate among the alloys. This is because the higher sliding speed increases frequency of cyclic stress. This may encourage breakage of the particulates by dislocation shearing under plastic deformation. At the same time, matrix oxidation, removal of the rapidly grown oxide film and subsurface matrix softening due to high frictional temperature conditions may also be effective. The increase of frictional energy consumed in the form of heat energy at higher sliding speeds softens the matrix. This may allow easier pull-out of carbide particles due to weakened interface. Thus, the wear rate of alloys increases with the sliding speed.

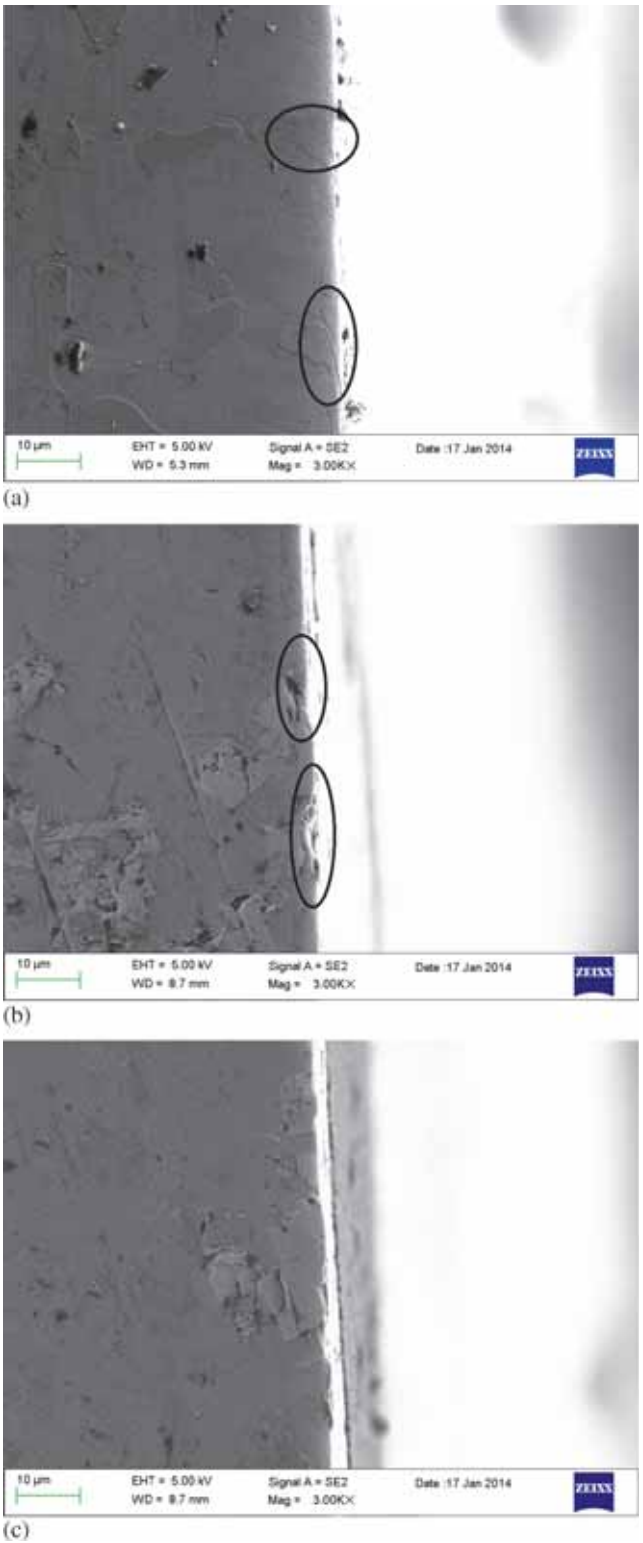

Figure 7. Cross-section of wear tracks of **(a)** Alloy-1, **(b)** Alloy-2 and **(c)** Alloy-3 showing different carbides embedded in matrix after sliding wear.

Figure 6 shows the coefficients of friction for all alloys tested at applied load of 10 N with sliding velocity

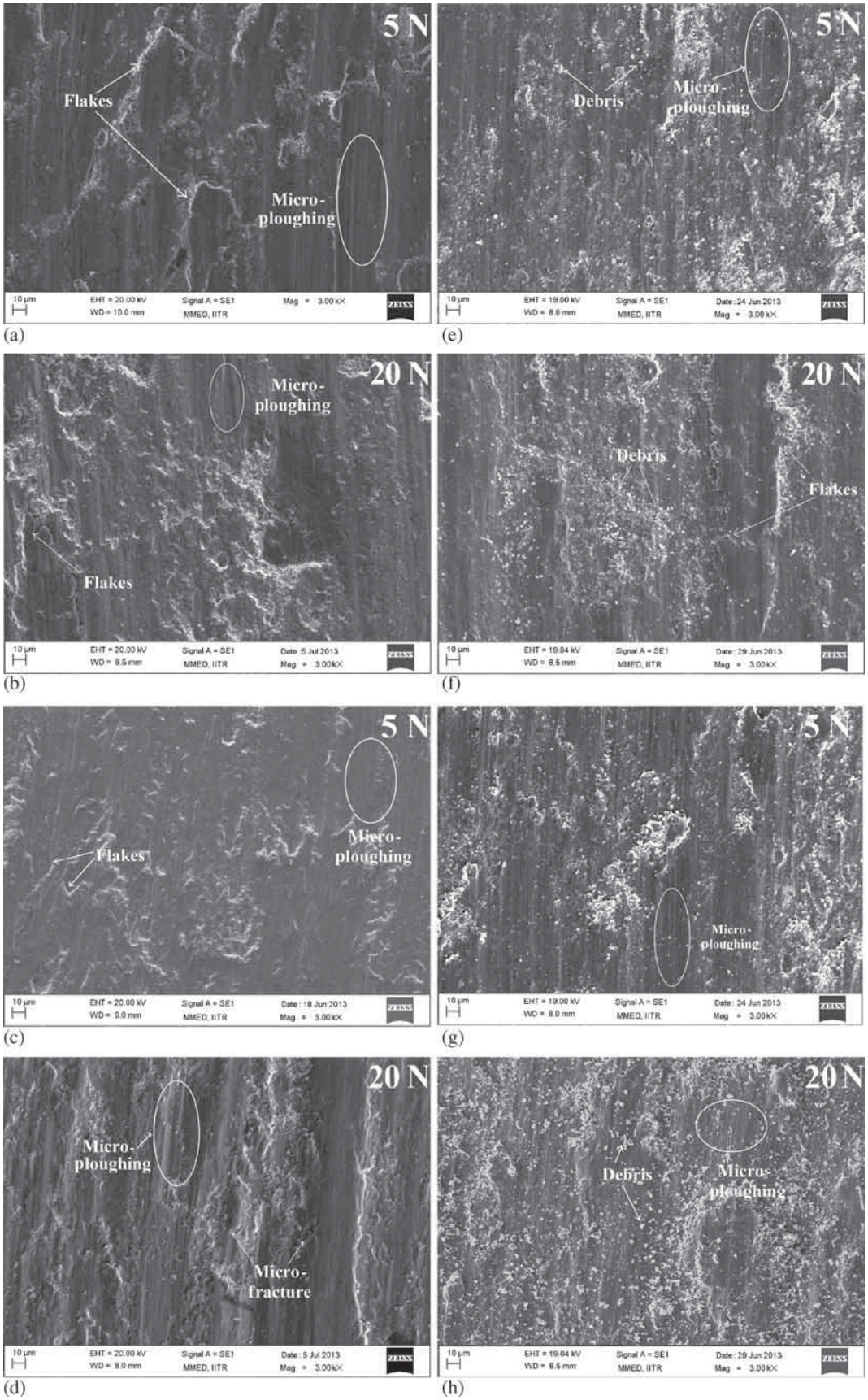

Figure 8. SEM micrographs showing morphologies of wear tracks for **(a, b)** Alloy-1, **(c, d)** Alloy-2, **(e, f)** Alloy-3 and **(g, h)** Alloy-4 at applied load 5 and 20 N with sliding speed 0.21 m s^{-1}.

0.21 m s^{-1}. The coefficient of friction increases sharply after initial fluctuations and acquires a relatively steady state, which prevails (figure 6). This indicates that hard carbide particles (ZrC in Alloy-2, TiC in Alloy-3 and Alloy-4) in matrix lower the shear and therefore contact area is much smaller. This leads to decrease in the coefficient of friction. Thus the coefficient of friction is strongly affected by the presence of hard ZrC and TiC carbides in FeAl-based alloys. It is well known that high friction coefficient results in higher wear rate [24].

Figure 7a shows the deformation of $Fe_3AlC_{0.5}$ carbide in sliding wear direction. Thus, deformation of $Fe_3AlC_{0.5}$ carbide would result in a higher friction coefficient of Alloy-1 than others. It may also be observed that the graphite flakes in Alloy-1 has lower load-bearing capacity. Thus, the deformation of $Fe_3AlC_{0.5}$ carbides in the sliding direction with a few graphite flakes enhanced the wear rate. On the other hand, the carbides such as ZrC and TiC in Alloy-2, Alloy-3 and Alloy-4 are embedded in the matrix even after sliding wear without any deformation. Figure 7b and c shows the cross-sectional area of the wear tracks of the alloys. It reveals that the carbides, mainly ZrC and TiC in Alloy-2 and Alloy-3, respectively, have very little effect of applied load. This strongly indicates that these carbides affect the wear rate of FeAl alloys without delamination or destruction while $Fe_3AlC_{0.5}$ carbide starts to deform in sliding direction under the applied load. This deformation of $Fe_3AlC_{0.5}$ carbides results in higher wear rate of Alloy-1.

Thus, the dispersion of carbides improves the wear resistance and friction coefficient of FeAl-based alloys. The hardness values of TiC or ZrC are significantly higher than that of $Fe_3AlC_{0.5}$ carbide. Also, no graphite precipitates are observed in these alloys (Alloy-2, Alloy-3 and Alloy-4). Therefore, the results demonstrate that uniform distribution of fine carbides in FeAl-based alloys works more effectively for wear resistance. These results also reflect that the wear rate of FeAl-based alloys decreased because different carbide particles play supporting role during the sliding wear. The microhardness difference between TiC and ZrC is not very large; thus wear rate should be similar. The compatibility issue among the matrix and the reinforcement plays an important role. TiC is found to be more compatible with FeAl matrix in comparison with ZrC [25]. This is due to the low CTE (coefficient of thermal expansion) mismatch between TiC and FeAl in comparison with ZrC and FeAl [25]. The observations clearly indicate that TiC is more compatible with FeAl matrix than ZrC. Also, most of the literature is on composites fabricated through PM route where bonding between matrix and ceramic particles is a major issue and leads to poor properties [26].

SEM micrographs of the wear tracks for different alloys are shown in figure 8. In general, the shear stress among the contact surfaces increased with increase in the applied load. A few lines in the friction surface with very small flakes would be initiated at lower applied load (figure 8a, c, e and g), while much more flakes would be produced and are more responsible for propagation at higher applied load (figure 8b, d, f and h). Thus, the wear rate in general of all alloys enhanced with increase in the applied load. The micrographs were taken after the sliding wear test conducted at different applied loads. In the mild testing conditions, i.e., low normal load and sliding speed, the surfaces show small flakes with fine debris and traces of microploughing were observed as shown in figure 8. However, in the severe conditions, i.e., at high normal load, the surface appearance was quite different. The wear surfaces were covered with deep grooves and flaking pits. The wear scars were heavily damaged, and the platelets and a trace of their detachment from the surface were observed together with the micro-ploughing.

During the sliding wear, the strains accumulate at the contacting points between the asperities, which subsequently form the surface deformation layers with increased dislocation density. The delamination is mainly due to cracking along the region of high dislocation density [27]. This effect is more pronounced in Alloy-2, Alloy-3 and Alloy-4 due to hard ZrC and TiC precipitates, respectively. Compared with $Fe_3AlC_{0.5}$, the higher hardness of both ZrC and TiC seems to play a positive role in resisting the wear damage from the counter-face and thus makes the process of delamination more difficult.

4. Conclusions

(1) The addition of transition alloying elements such as Zr and Ti to FeAl-based alloys containing carbon resulted in increase in the strength and hardness. This increase is mainly attributed to the precipitation of hard carbides (ZrC/TiC). Zr addition results in precipitation of hard ZrC and Laves phase $Zr(FeAl)_2$. Ti addition causes precipitation of hard TiC. No graphite precipitation was observed in FeAl-based alloys on Zr and Ti addition.
(2) With addition of Ti and Zr, the coefficient of friction and wear rate of FeAl-based alloys decreased due to higher hardness of TiC and ZrC, respectively.
(3) Wear mechanism of FeAl-based alloys was transferred from the micro-ploughing to micro-fracture and their detachment from the surface with applied load and sliding speed.
(4) The hardness, strength and wear rate of these alloys are determined by the volume fraction and hardness of carbides present.
(5) The *in-situ* production of carbides provides good bonding between the carbides and matrix and hence improves the wear resistance of FeAl alloys as compared with composites of iron aluminides mostly prepared using the powder metallurgy route.

Acknowledgement

This research has been supported by the Department of Science and Technology, New Delhi, and we are thankful for the financial support.

References

[1] Deevi S C and Sikka V K 1996 *Intermetallics* **4** 357

[2] Mckamey C G and Stoloff N S 1996 in: *Physical metallurgy and processing of intermetallic compounds* (eds) N S Stoloff and V K Sikka p 351

[3] Prakash U 2008 *Trans. Indian Inst. Met.* **61** 193

[4] Prakash U and Sauthoff G 2001 *Scr. Mater.* **44** 73

[5] Sundar R S and Deevi S C 2003 *Metall. Mater. Trans. A* **34** 2233

[6] Alman D E, Hawk J A, Tylczak J H, Dogan C P and Wilson R D 2001 *Wear* **251** 875

[7] Radhakrishna A, Baligidad R G and Sarma D S 2001 *Scr. Mater.* **45** 1077

[8] Kopecek J, Hausild P, Jurek K, Jarosova M, Drahokoupil J, Novak P and Sima V 2010 *Intermetallics* **18** 1327

[9] Kuzucu V, Aksoy M and Korkut M H 1998 *J. Process. Technol.* **82** 165

[10] Kant R, Prakash U, Agarwala V and Satyaprasad V V 2015 *Trans. Indian Inst. Met.* doi: 10.1007/s12666-015-0567-z

[11] Guan X, Iwasaki K, Kishi K, Yamamoto M and Tanaka R 2004 *Mater. Sci. Eng. A* **366** 127

[12] Kant R, Prakash U, Agarwala V and Satyaprasad V V 2015 *Intermetallics* **61** 21

[13] Zhang X, Ma J, Yang J, Bi Q and Liu W 2011 *Wear* **271** 881

[14] Palm M and Sauthoff G 2004 *Intermetallics* **12** 1345

[15] Stein F, Sauthoff G and Palm M 2004 *Z. Metallkd.* **95** 469

[16] Kratochvila P, Dobes F, Pesicka J, Malek P, Bursik J, Vodickova V and Hanus P 2012 *Mater. Sci. Eng. A* **548** 175

[17] Hawk J A and Alman D E 1993 *Wear* **225–229** 544

[18] Mosbah A Y, Wexler D and Calka A 2005 *Wear* **258** 1337

[19] Subramanian R and Schneibel J H 1998 *Mater. Sci. Eng. A* **244** 103

[20] Aikin R M 1997 *J. Min. Met. Mater. Soc.* **49** 35

[21] Raghunath C, Bhat M S and Rohatgi P K 1995 *Scr. Metall.* **32** 577

[22] Terry B S and Chinyamakobvu O S 1991 *J. Mater. Sci. Lett.* **10** 628

[23] Palm M 2005 *Intermetallics* **13** 1286

[24] Qiu J, Baker I, Kennedy F E, Liu Y and Munroe P R 2013 *Intermetallics* **40** 19

[25] Houska C R 1964 *J. Phys. Chem. Solids* **25** 359

[26] Subramanian R and Schniebel J H 1997 *J. Min. Met. Mater. Soc.* **49** 50

[27] Kim Y S and Kim Y H 1998 *Mater. Sci. Eng. A* **258** 319